1   **Anatomy of unfolding: The site-specific fold stability of Yfh1 measured by 2D NMR**

2

3   Rita Puglisi, Annalisa Pastore*, Piero Andrea Temussi*

4   UK-DRI at King's College London, The Wohl Institute, 5 Cutcombe Rd, SE59RT London

5   (UK)

6

7

8   *To whom correspondence should be addressed

9   annalisa.pastore@crick.ac.uk

10   temussi@unina.it

11

12   **Keywords:** biophysics, cold denaturation, NMR, protein stability, thermal unfolding,

13   thermodynamics

14   **Running title:** Site specific fold stability of Yfh1 by 2D NMR

15

16

Abstract

Most techniques allow detection of protein unfolding either by following the behaviour of single reporters or as an averaged all-or-none process. We recently added 2D NMR spectroscopy to the well-established techniques able to obtain information on the process of unfolding using resonances of residues in the hydrophobic core of a protein. Here, we questioned whether a detailed analysis of the individual stability curves from each resonance could provide additional site-specific information. We used the Yfh1 protein that has the unique feature to undergo both cold and heat denaturation at temperatures above water freezing at low ionic strength. We show that stability curves inconsistent with the average NMR curve from hydrophobic core residues mainly comprise exposed outliers that do nevertheless provide precious information. By monitoring both cold and heat denaturation of individual residues we gain knowledge on the process of cold denaturation and convincingly demonstrate that the two unfolding processes are intrinsically different.

30

31

MAGNETIC RESONANCE
Open Access
Discussions

32 **Introduction**

33 Most techniques employed to monitor protein stability are not "regiospecific", as they yield a

34 global result, i.e. an estimate of the stability of the whole protein architecture, observable

35 through the global evolution of secondary structure elements upon an environmental insult.

36 This is because we postulate an all-or-none cooperative process in which the protein collapses

37 altogether from a folded to an unfolded state. When monitoring the unfolding of a protein by

38 CD spectroscopy, for instance, we observe intensity changes related to the disruption of α

39 helices and/or β sheets under the influence of physical or chemical agents.

40   It is nevertheless interesting to gauge the response of selected regions of the protein or

41 even single residues during the unfolding process to gain new insights into the mechanisms of

42 unfolding in selected parts of the protein structure. A technique ideally suited for this purpose

43 is 2D NMR spectroscopy since it permits to monitor changes in the resonances at the level of

44 individual residues. Particularly suitable are 2D ^{15}N HSQC spectra since they provide a direct

45 fingerprint of the protein through mapping each of the amide protons. Volume variations of the

46 NMR resonances may reflect changes affecting single atoms of each residue and indirectly

47 report on how they are individually affected by the unfolding process. We have recently shown

48 that it is possible to use 2D NMR to measure protein stability and get thermodynamics

49 parameters comparable to those obtained by standard CD methods, provided that a suitable

50 selection of the residues is made, followed by the subsequent average of the changes of these

51 residues (Puglisi et al., 2020). To choose residues whose NH is deep inside the protein and

52 relatively inaccessible to the solvent we employed SADIC (Varrazzo et al., 2005), a software

53 that quantifies depth inside the protein (D), in combination with PopS (Cavallo et al, 2003) that

54 yields relative accessibility at an atomic level (RA). We combined the two parameters defining

55 a new parameter, RAD, which combines depth and exposure. We demonstrated that the

56 stability curve calculated from averaging amide volumes from residues with a RAD value

57 below 0.1 (here henceforth called RAD_0.1) is consistent with that calculated from CD

58 spectroscopy (Puglisi et al., 2020).

59   It is now interesting to wonder what information is carried by residues far from the

60 hydrophobic core and how they reflect the process of unfolding. This is relevant also in view

61 of an increasing number of studies on protein stability based on the intensity variations of the

62 resonance of a single residue upon unfolding (Danielsson et al., 2015; Smith et al., 20116;

63 Guseman et al., 2018). The excellent agreement between NMR and CD thermodynamic

64 parameters (Puglisi et al., 2020) put us in the position to examine the output of single residues

65 critically, and eventually follow the process of unfolding at an atomic level.

MAGNETIC RESONANCE Discussions

66   Here, we present the analysis of the stability of the yeast ortholog, Yfh1, of human frataxin as

67   measured by the stability curves of most observable, isolated NH resonances. We chose Yfh1

68   to probe regiospecific unfolding because this protein is an ideal model system for measuring

69   stability curves of single residues: in addition to heat denaturation, Yfh1 has a cold denaturation

70   temperature observable above zero degrees when in the absence of salt (Pastore et al., 2007).

71   Observation of the two unfolding temperatures facilitates enormously the calculation of reliable

72   stability curves and of the whole set of thermodynamic parameters. The usefulness of Yfh1 as

73   a tool to investigate unfolding processes is evidenced not only by our subsequent work (Pastore

74   et al., 2007; Sanfelice et al., 2013; Pastore and Temussi, 2017; Martin et al., 2008; Sanfelice et

75   al., 2014; Alfano et al., 2017) but also by papers from other laboratories (Espinosa et al., 2016;

76   Chatterjee et al., 2014; Bonetti et al., 2014; Aznauryan et al., 2013).

77   We demonstrate that it is possible to sort out which individual single residues yield

78   stability curves consistent with the global unfolding process and that we can obtain valuable

79   information on the process of unfolding from residues that diverge from the average behaviour,

80   Our data also prove directly the distinct mechanisms determining the cold and heat denaturation

81   processes by providing site-specific information on solvent interactions.

82

83   **Results**

84   We collected ^{15}N HSQC spectra of Yfh1 at different temperatures and from them plotted the

85   volumes of individual residues as a function of temperature. It is possible to extract

86   thermodynamic parameters from these plots provided some conditions are met (Privalov, 1990;

87   Martin et al., 2008). It is first assumed that unfolding transitions are two-state processes from

88   folded (F) to unfolded (U) states. It is then hypothesized that the difference of the heat capacity

89   of the two forms (ΔC_p) does not depend on temperature. This assumption is considered

90   reasonable when the heat capacities of the native and denatured states change in parallel with

91   temperature variation (Privalov, 1990). When these conditions are true, the populations of the

92   two states at temperature T, $f_F(T)$ and $f_U(T)$, can be expressed as a function of the difference in

93   free energy, $\Delta G^o(T)$, according to the modified Gibbs-Helmholtz equation (Martin et al., 2008).

94   The curve corresponding to this equation is known as the stability curve of the protein (Becktel

95   and Schellman, 1987). The main thermodynamic parameters, T_m, ΔH_m and ΔC_p, can be

96   determined using a non-linear fit (damped least-squares method). Other parameters for low

97   temperature unfolding, e.g. T_c, can be read from the stability curve. Volumes of isolated

98   residues were transformed into relative populations of folded Yfh1 assuming that, as found in

99   other studies on Yfh1 (Pastore et al., 2007; Martin et al., 2008; Sanfelice et al., 2014; Alfano

100   et al., 2017), unfolded forms are in equilibrium with a 70% population of folded Yfh1 at room

101   temperature (**Table 1**). The concurrent presence of an equilibrium between folded and

102   unfolding species is directly testified by the spectra at low ionic strength: folded and well

103   dispersed resonances co-exist with others strongly overlapping. These extra peaks disappear as

104   soon as physiologic concentrations of NaCl are added (Vilanova et al., 2014).

105   We then correlated each amide resonance to the corresponding value of RAD, the

106   parameter introduced in Puglisi et al. (2020), to pinpoint residues close to the hydrophobic

107   core. The behaviour of resonances in the HSQC spectrum of Yfh1 as a function of temperature

108   was also not uniform. While some peaks could be observed nearly at all temperatures in the

109   range 273-323 K, others disappeared at temperatures intermediate between room temperature

110   and the two unfolding temperatures, i.e. lower than 323 K or higher than 273 K (**Figure S1 of**

111   **Suppl. Mat.**). This behaviour was of course related to the exchange regime of these residues

112   and told us that they are not an integral part of the architecture of the folded form and thus their

113   volume variations cannot represent the all-or-none overall unfolding process faithfully. It was

114   anyway possible to calculate a stability curve from the temperature dependence of the

115   resonance volumes and the corresponding thermodynamic parameters for many residues, to

116   yield valuable information on the unfolding process. We then looked into what these residues

117   could tell us about the unfolding process.

118

Residues consistent with or outliers from the global behaviour

119

120   Comparison of the stability curves of all the well behaved residues (68 over the expected 109

121   resonances) with the average best curves calculated for RAD values <0.1 (henceforth called

122   RAD_0.1) showed that several residues yield stability curves drastically different from the

123   average curve (**Figures 1a**). The curves for residues in the hydrophobic core are overall in good

124   agreement with the best average curve (**Figures 1b**). However, there is in principle no clear-

125   cut criterion to decide when the curves are not consistent with the average. We arbitrarily chose

126   to set a cut-off at values of the unfolding temperatures (T_m and T_c) that differed, on average,

127   less than 1.5 K from those corresponding to the average (RAD_0.1). This difference is smaller

128   than the variability that we had observed among different preparations and measurements of

129   the same protein (Pastore et al., 2007; Martin et al., 2008; Sanfelice et al., 2014; Sanfelice et

130   al., 2015; Alfano et al., 2017; Puglisi et al., 2020). The residues selected according to this

131   criterion are E71, E75, E89, L91, D101, L104, S105, M109, T110, F116, Y119, I130, L132,

132   A133, F142, D143, L152, L158, T159, D160, T163, and K168 (**Figure 1c**). Most of the amide

133   groups of the well-behaved residues are spread among well-structured secondary elements, but

134   there are a few in less ordered regions (**Figure 2a**). By the same token, we selected as 'ill-

135   behaved' residues those whose ΔT_m and ΔT_c were greater, on average, than 3 K with respect

136   to the best curve (RAD_0.1). Eighteen residues (V61, Q63, H83, H95, C98, G107, V108, I113,

137   V120, N127, K128, Q129, L136, N146, G147, N154, K172, Q174) belong to this sub-set.

138   Similarly, except for a few outliers, they all are in less structured regions (**Figure 2b**).

139

140
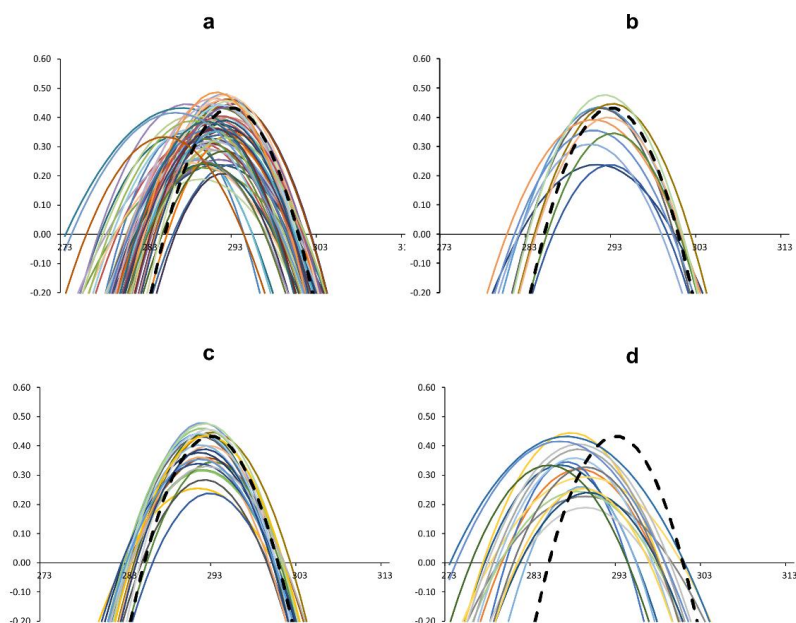
Figure 1. Comparison of single residue stability curves with the global (RAD_0.1) best curve
(dashed black). **a**) Stability curves of all observable isolated residues. **b**) Stability curves of
residues with a RAD<0.1. **c**) Stability curves of single residues for which the difference in the
unfolding temperatures with respect to values of the reference curve (ΔT_m and ΔT_c) is on
average below 1.5 °C **d**) Stability curves of single residues for which the difference in the
unfolding temperatures with respect to values of the average curve (ΔTm and ΔTc) is on
average above 3 K.

149   The stability curves of these residues (**Figure 1d**) have an important peculiarity: most stability

150   curves show a moderate decrease of T_m and a large decrease of T_c. This finding is paradoxical

151   because it implies that the corresponding transition temperatures for the heat and cold unfolding

152   point to decreased and increased stability for heat and cold denaturation respectively. Although

153   it is difficult to explain the behaviour of the extreme values of the ΔT_c of some residues, it is

154   fair to say that this behaviour confirms that the mechanisms of the two unfolding processes are

155   intrinsically different. This possibility was already postulated by Privalov (Privalov, 1990) who

156   suggested that the disruption of the hydrophobic core at low temperature would be caused by

157   the hydration of the side chains of hydrophobic residues of the core, whereas the high

158   temperature transition is mainly linked to entropic reasons, consistent with the increase of

159   thermal motions when temperature is increased. What we observed is also in line with our

160   previous evidence that showed that the unfolded species at low temperature has a volume

161   higher than the folded species and of the high temperature unfolded species (Alfano et al.,

162   2017) and that cold denaturation is caused by a hydration increase (Adrover et al., 2012).

163   In light of this fundamental difference, it is tempting to hypothesize that the large ΔT_c of

164   residues positioned in the middle of connecting turns, G107, N127, N146 and N154 (**Figure**

165   **2c),** may reflect the fact that these flexible (well hydrated) structural elements keep some

166   resilience since they do not experience environmental changes even after the core has been

167   invaded by water molecules and are the last to be affected by unfolding.

168

169
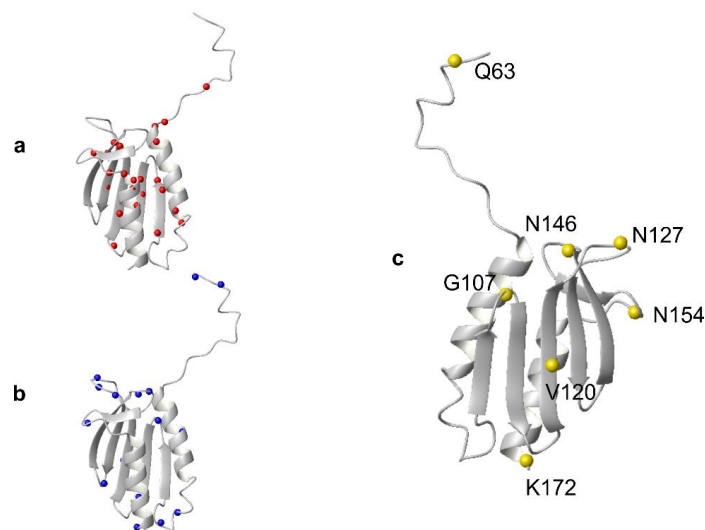
Figure 2. Distribution of residues on the structure of Yfh1. a) Distribution of the N atoms of
residues for which the difference in the unfolding temperatures with respect to values of the
RAD_0.1 curve (ΔTm and ΔTc) is on average below1.5 K. b) Distribution of the N atoms of
residues for which the difference in the unfolding temperatures with respect to values of the
average curve (ΔTm and ΔTc) is on average above 3 K. c) The gold dots on the structure mark
the positions of residues whose stability curve is most shifted to lower temperatures with
respect to the average one (RAD_0.1).

177

178   In other words, these residues seem to form a kind of exoskeleton that is tougher at lower

179   temperatures. This view is consistent with the observation that, when decreasing the

180   temperature towards the cold denaturation transition there is a decrease of thermal motions that

181   may favour the persistence of structural elements less ordered than helices and beta sheet.

182

A thermodynamic assessment of flexibility

184   The negative ΔT_m and ΔT_c observed for some residues (**Figure 1d**) imply that the temperature

185   of maximum stability (T_S, so called because it corresponds to zero entropy) is lower than that

186   observed for the best average (RAD_0.1). The low temperature shift of T_S values is consistent

187   with the unfolding of more flexible parts of the protein structure because it corresponds to an

188   increase in entropy connected to unfolding.

189
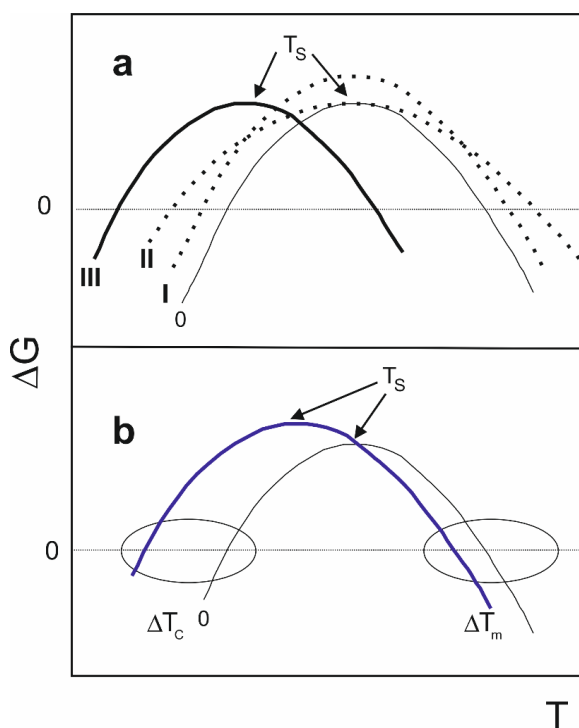
Figure 3. Mechanisms that influence stability curves of a protein (adapted from Nojima et al, 1977). **a**) Dependence of the difference of free energy between unfolded and folded states (ΔG) of a hypothetical protein vs temperature (curve 0). Mechanism I illustrates the effect of increasing ΔH_S (curve I). Mechanism II shows the effect of reducing ΔC_p (curve II). Mechanism III shows the shift of the whole stability curve towards lower temperatures caused by increasing ΔS_m (curve III). **b**) A combination of the three mechanisms. The solid blue curve corresponds qualitatively to the cases of Yfh1 reported in **Figure 1 d**.

198

199   This consideration (Razvi & Scholtz, 2006) is based on the classification by Nojima et

200   al. (1977) of the main mechanisms of changing the thermal resistance of a protein.

201   Obviously, the same holds true if one wants to *decrease* T_m or T_c: it is sufficient to reverse the

202   changes. According to the rough classification of Nojima et al. (1977), altered thermostability

203   can be achieved thermodynamically in three different ways (**Figure 3**).

204   According to mechanism (I), when ΔH_S (the change in enthalpy measured at T_S) increases, the

205   stability curve retains the same shape, but with greater ΔG values at all temperatures. With

206   mechanism II, a decreased ΔC_p leads to a broadened stability curve, because the curvature of

207   the stability curve is given (Becktel, & Schellman, 1987) by $\dfrac{\partial^2 \Delta G}{\partial T^2} = -\dfrac{\Delta C_p}{T}$. According to

208   mechanism III, the entire curve can shift towards higher or lower temperatures. It is possible

209   to show (Privalov, 1990) that:

210
$$T_S = T_m \cdot \exp\left[-\frac{\Delta S_m}{\Delta C_p}\right] = T_m \cdot \exp\left[-\frac{\Delta H_m}{T_m \cdot \Delta C_p}\right].$$

211   Increasing the difference in entropy between the folded and unfolded states (ΔS_m) can shift

212   values of T_S towards lower temperatures. Most of the curves of **Figure 1d** do not correspond

213   to a single mechanism, but to a combination of them (**Figure 3b**). However, all are shifted

214   toward lower values of T_S. The largest low-temperature differences correlate well with less

215   ordered regions of the structure. These regions experience largest unfolding entropies and thus

216   visit a larger number of conformations. It is not surprising to find this behaviour for residues

217   at the N- and C-termini (Q63 and K172) or in connecting loops (G107, N127, N146 and N154)

218   which are bound to be flexible (Halle, 2002). More surprising is, however, to find amongst

219   these residues also V120 which is right in the middle of the β-sheet. While we have not a

220   definite explanation for this observation at the moment, it could indicate a local frustration

221   point in this region.

222

223   **Exploring the correlation between stability and secondary structure elements**

224   We have previously shown that, in addition to the criteria of depth and exposition, an

225   alternative selection of residues over which average populations might be based on elements

226   of regular secondary structure (Puglisi et al., 2020). It is now possible to analyse the behaviour

227   of each secondary structure element. The stability curves related to accessible residues of

228   individual secondary structure elements are summarized in **Figures 4** and **5**. The largest

229 number of residues of secondary structure traits whose resonance is accessible belongs to the

230 two helices (**Figure 4**).

a

b

231
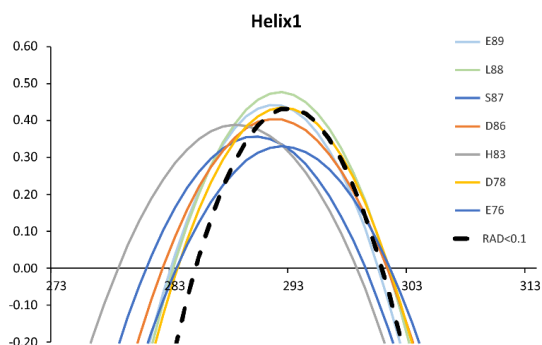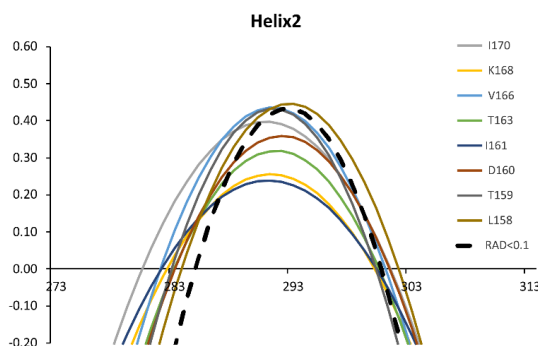
Figure 4. Stability curves of residues belonging to secondary structure elements. **a**) Helix 1.
b) Helix 2. Residues are labelled with single letter code. The average stability curve is shown
as black dashed line.

236 Both for helix 1 (**a**) and helix 2 (**b**) there are several resonances whose stability curve is far

237 from the reference one (dashed black curve of RAD_0.1). In particular, these are those of His83

238 and Ser87 for helix 1. All the others are in fair agreement with the average curve. The best

239 behaved residues (Glu76, Asp78, Leu88 and Glu89) are located at the two ends of the helix

240 with their amide groups in the buried side of the helix. For helix 2, the worst agreement is found

241 for Ile161 and Ile170, whereas the best agreement is for Leu158, Thr159, Asp160, Thr163 and

242 Lys168. This implies that residues of helix 2 with a good agreement are distributed over the

243 whole secondary structure element.

244   The number of residues belonging to beta strands for which it was possible to extract

245 stability curves is more limited (**Figure 5**).

10

246
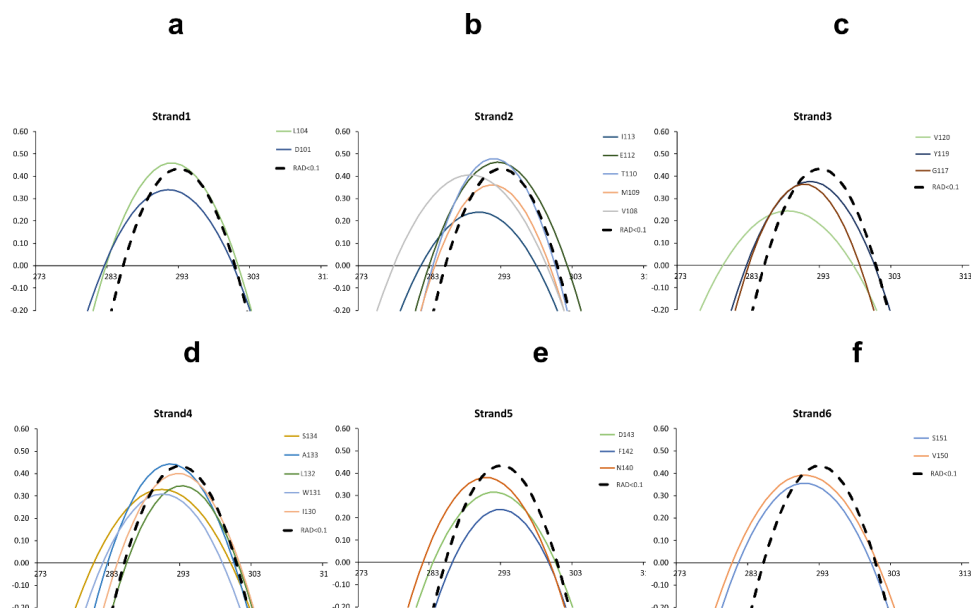
Figure 5. Stability curves of residues belonging to secondary structure elements. a) Strand 1.
b) Strand 2. c) Strand 3. d) Strand 4. e) Strand 5. f) Strand 6. Residues are labelled with single
letter code. The average stability curve is shown as black dashed line.

The best agreement was found for Leu104 of strand 1, Met109 and Thr110 of strand 2, Ile130,

Leu132 and Ala133 of strand 4 and Phe142 and Asp143 of strand 5. It is interesting to note

that some of the best residues reported in **Figure 1c** are not present in regular secondary

structure elements.

The behaviour of tryptophan side chains

We then looked into the possibility of following the process of unfolding and calculating

thermodynamic parameters using the tryptophan side chains. This choice directly parallels

studies based on following the process of unfolding by fluorescence using the intrinsic

tryptophan fluorescence (Monsellier & Bedouelle, 2002). Yfh1 has two tryptophans: W131 is

fully exposed to the solvent whereas W149 is buried. Both residues are fully conserved

throughout the frataxin family and the two side chain resonances are clearly identifiable

(**Figure S2a of Suppl. Mat.**). We calculated the thermodynamic parameters for the side chain

indole groups of both residues (**Table 1**) by the same procedure outlined for main chain NHs,

generating first a stability curve (**Figure S2b of Suppl. Mat.**). The resonance of W149, which

could potentially be more interesting, could not be used for quantitative measurements because

268 the temperature dependence of its volume yields a stability curve very different from the others

269 (**Figure S2b of Suppl. Mat.**) which leads to impossible parameters. This might be explained

270 by the co-existence of folded and partially unfolded species in equilibrium with each other in

271 solution. As a consequence the indole of W149 resonates both at 9.25 and 127.00 ppm (folded

272 specie) and at ca. 10.05 and 129.20 ppm (split into three closely adjacent peaks, unfolding

273 intermediates) (**Figure S2a of Suppl. Mat.**). As previously proven experimentally, the

274 resonances of the unfolding intermediates disappear upon addition of salt (Figure 1, panel A

275 and B in Vilanova et al., 2014). These resonances are also at the same coordinates observed for

276 the tryptophan indole groups at low and high temperature where however the three species

277 collapse into one (**Figure S1 of Suppl. Mat.**). The complex equilibrium between different

278 species could thus explain the ill-behaviour of the corresponding stability curve of this residue.

279 The behaviour of the resonance of the exposed W131 side chain is instead fully consistent with

280 that of RAD_0.1 and also with the original curve calculated from 1D NMR data (Pastore et al.,

281 2007). On the whole, these results exemplify well the complexity of the selection choice of the

282 unfolding reporter and advocate in favour of a wholistic analysis of the whole set of available

283 data.

284

285 **Discussion**

286 The *de facto* demonstration that it is possible to reliably measure the thermodynamic

287 parameters of protein unfolding by 2D NMR spectroscopy (Puglisi et al., 2020) has opened a

288 new territory to study protein unfolding at atomic resolution using site-specific information.

289 Following protein folding/unfolding looking at specific residues rather than obtaining an

290 average overall picture is not a novelty. Despite some intrinsic limitations, fluorescence has,

291 for instance, been used for decades to probe protein unfolding following the intrinsic

292 tryptophan fluorescence (Monsellier & Bedouelle, 2002; Bolis et al., 2004). Another elegant,

293 although sadly still underexploited technique able to report local behaviour at the level of

294 specific residues is chemically induced dynamic nuclear polarization (CIDNP) first introduced

295 to the study of proteins by Robert Kaptein (Kaptein et al., 1978). This technique allows the

296 selective observation of exposed tryptophans, histidines and tyrosines. In protein folding, it

297 was, for instance, used to characterize the unfolded states of lysozyme (Broadhurst et al., 1991;

298 Schlörb et al., 2006) and the molten globule folding intermediate of α-lactalbumin (Improta et

299 al., 1995; Lyon et al., 2002). Real-time CIDNP was also used to study the refolding of

300 ribonuclease A (Day et al., 2009) and HPr (Canet et al., 2003). The only drawback of this

301 technique is that, as in fluorescence, the information is limited to specific aromatic residues.

302   Another important technique that reports on protein unfolding at the single residue level

303   is stopped-flow methods coupled with NMR measurements of hydrogen exchange (Kim and

304   Baldwin, 1991; Roder and Wüthrich, 1986) and by mass spectrometry (Miranker et al., 1993).

305   In a classic paper (Miranker et al., 1991), Dobson and co-workers described, for instance, NMR

306   experiments based on competition between hydrogen exchange as observed in COSY spectra

307   and the refolding process. The authors could conclude in this way that the two structural

308   domains of lysozyme followed two distinct folding pathways, which significantly differed in

309   the extent of compactness in the early stages of folding. Similar and complementary

310   conclusions could be reached by integrating NMR with mass spectrometry (Miranker et al.,

311   1993). While these studies retain their solid importance, the possibility of following the

312   resonance intensities also by HSQC spectra may provide a more flexible tool to obtain detailed

313   information on unfolding as it reports on the exchange regime but also, implicitly, on the

314   chemical environment. The use of 2D HSQC had been discouraged by the non-linear

315   relationship between peak intensity (or volume) and the populations with temperature as the

316   consequence of relaxation, imperfect pulses, and mismatch of the INEPT delay with specific

317   J-couplings. We have previously suggested an approach to compensate for these effects and

318   demonstrated that the non-linearity does not affect the spectra of Yfh1 (Puglisi et al., 2020),

319   even though these conclusions might be protein dependent.

320   Here, we reconsidered our previous work (Puglisi et al., 2020) and measured individual

321   stability curves for most of the residues of Yfh1. Our approach showed to be particularly

322   fruitful for the study of this protein that has an unusual if not unique behaviour since, as a

323   natural unmodified full-length protein, it undergoes cold and heat denaturation when in the

324   absence of salts, allowing measurement of the whole stability curve. The availability of this

325   model system permitted us to shed light onto several important aspects.

326   We observed that the behaviour of the individual stability curves is not distributed

327   uniformly along the sequence. Residues can be clearly divided into two groups, i.e. those

328   consistent with the average behaviour of an all-or-none mechanism of unfolding and those

329   differing, even strongly, from the best average (RAD_0.1). This finding alone proved that it is

330   not possible to measure stability using a single residue without a careful evaluation of the role

331   of the specific residue in the protein fold. This conclusion is partially mitigated by our results

332   on the parameters obtained for a tryptophan indole. However, in the whole, also for these side

333   chains it may be difficult, *a priori,* to infer which tryptophan is more reliable, thus suggesting

334   that unfolding studies based on fluorescent measurements using the intrinsic fluorescence of

335   tryptophan should be taken with a pinch of salt. Even though our findings support the

MAGNETIC
RESONANCE
Discussions

336   possibility of obtaining protein stability parameters using the intrinsic tryptophan fluorescence
337   data in our specific example, in many other cases no independent controls could be done to
338   evaluate the accuracy of the results. The possibility of using 2D NMR and the introduction of
339   the easily approachable RAD parameter may assist in this choice in future studies.

340   Analysis of individual secondary structure elements, i.e. helices and strands, showed that
341   there is no clear hierarchy among them, and there is no indication that any of the elements
342   undergoes disruption before the others, either at high or at low temperature. It will be
343   interesting in the future to study lysozyme to have an example in which two subdomains unfold
344   independently (Miranker et al., 1991). In addition to information on regular secondary structure
345   elements, our analysis yielded also interesting information on less ordered traits. Intrinsically
346   flexible elements, i.e. regions characterized by multiple conformers, can be identified
347   unequivocally by their thermodynamic parameters, without recurring to interpretative
348   mechanisms.

349   Another important point is that we observed a clear difference between parameters
350   corresponding to the cold and the heat denaturation processes: residues that are outliers from
351   the average stability curve tend to have a strong stabilization effect at low temperature and a
352   weak destabilising effect at high temperature. This is a strong confirmation that the
353   mechanisms of the two transitions are intrinsically different according to the mechanism of
354   cold unfolding proposed by Privalov. In this model, cold denaturation is intimately linked to
355   the hydration of hydrophobic residues of the core (Privalov, 1990; Adrover et al., 2012). One
356   outstanding consequence is that, at the temperature of global unfolding, corresponding to that
357   of the average of the deeply buried protein core (RAD_0.1), residues outside the hydrophobic
358   core and in regions classified as flexible may be more resilient against unfolding. In other
359   words, at low temperature, opening of the hydrophobic core and its disruption can happen
360   before the collapse of external and more exposed elements.

361   In conclusion, we can state that monitoring protein degradation by individual residue
362   stability curves, as allowed by 2D NMR spectroscopy, yields a much more informative picture
363   than what may be obtained by traditional methods, particularly when both cold and heat
364   unfolding can be observed.

365

366   **Methods**

367   *Sample preparation*

14

368 Yeast frataxin (Yfh1) was expressed in BL21(DE3) *E. coli* as previously described (Pastore et
369 al., 2007). To obtain uniformly ^{15}N-enriched Yfh1, bacteria were grown in M9 using ^{15}N-
370 ammonium sulphate as the only source of nitrogen until an OD of 0.6-0.8 was reached and
371 induced for 4 hours at 310 K with 0.5 mM IPTG. Purification required two precipitation steps
372 with ammonium sulphate and dialysis followed by anion exchange chromatography using a Q-
373 sepharose column with a NaCl gradient. After dialysis the protein was further purified by a
374 chromatography using a Phenyl Sepharose column with a decreasing gradient of ammonium
375 sulphate.

376

377 *NMR measurements*
378 2D NMR ^{15}N-HSQC experiments were run on a 700 MHz Bruker AVANCE spectrometer.
379 Following the strategy previously described (Puglisi et al., 2020), ^{15}N-labelled Yfh1 was
380 dissolved in 10 mM Hepes at pH 7.5 to reach 0.1 mM. Spectra were recorded in the range 5-
381 40 ºC with intervals of 2.5 ºC and using the Watergate water suppression sequence (Piotto et
382 al., 1992). For each increment 8 scans were accumulated, for a total of 240 increments. Spectra
383 were processed with NMRPipe and analysed with CCPNMR software. Gaussian (LB -15 and
384 GB 0.1) and cosine window functions were applied for the direct and indirect dimension
385 respectively. The data were zero-filled twice in both dimensions. Spectral assignments of Yfh1
386 correspond to the BMRB deposition entry 19991.

387

388 **Selection of the best set of amides**
389 Yfh1 contains 114 backbone amide protons. The first 23 residues are an intrinsically sequence
390 that contains the region for mitochondrial import and processing, leading to 91 resonances in
391 the globular domain. 68 have non-overlapping and isolated resonances that allow easily
392 detectable and reliable volume calculation. Most of the excluded overlapping resonances
393 corresponded to disordered regions or to a partially unfolded conformation in equilibrium with
394 the folded one in a slow exchange regime at room temperature (Sanfelice et al., 2014).
395 Volumes were calculated by summation of intensities in a set box using the CCPNMR software.
396 The parameter RAD was used taking the parameters from the software Pops
397 (http://mathbio.nimr.mrc.ac.uk/~ffranca/POPS)   and   SADIC
398 (http://www.sbl.unisi.it/prococoa/).
399 Residues involved in secondary structures were evaluated according to the DSSP program
400 (https://swift.cmbi.umcn.nl/gv/dssp/). This software is all freely available. Our analysis
401 resulted in 35 residues in secondary structure elements (15 in alpha helices, 20 in beta sheets),

402   39 residues having RAD <0.5, 37 with RAD <0.4, 33 with RAD <0.3, 24 with RAD <0.2 and

403   11 having RAD < 0.1 (Puglisi et al., 2020).

404

405   **AUTHOR INFORMATION**

406   **Corresponding authors**

407   annalisa.pastore@crick.ac.uk

408   temussi@unina.it

409

410   **Acknowledgments**

420

421

References

Adrover M, Martorell G, Martin SR, Urosev D, Konarev PV, Svergun DI, Daura X, Temussi P, Pastore A. The role of hydration in protein stability: comparison of the cold and heat unfolded states of Yfh1. J Mol Biol. 2012 Apr 13;417(5):413-24. doi: 10.1016/j.jmb.2012.02.002.

Alfano, C., Sanfelice, D., Martin, S. R., Pastore, A. and Temussi, P. A.: An optimized strategy to measure protein stability highlights differences between cold and hot unfolded states, Nat. Commun., 8, 15428, 2017, doi: 10.1038/ncomms15428.

Aznauryan, M., Nettels, D., Holla, A., Hofmann, H. and Schuler, B. Single-molecule spectroscopy of cold denaturation and the temperature-induced collapse of unfolded proteins. J. Am. Chem. Soc. 135, 14040-3, 2013, doi: 10.1021/ja407009w.

Becktel, W. J. and Schellman, J. A.: Protein stability curves, Biopolymers, 26, 1859-77, 1987, doi: 10.1002/bip.360261104.

Bolis, D., Politou, A. S., Kelly, G., Pastore, A. and Temussi, P. A. Protein stability in nanocages: a novel approach for influencing protein stability by molecular confinement. J. Mol. Biol., Feb 6;336(1):203-12, 2004, doi:10.1016/j.jmb.2003.11.056.

Bonetti, D., Toto, A., Giri, R., Morrone, A., Sanfelice, D., Pastore, A., Temussi, P., Gianni, S. and Brunori, M. The kinetics of folding of frataxin. Phys. Chem. Chem. Phys., 16, 6391-7, 2014, doi: 10.1039/c3cp54055c.

Broadhurst, R.W., Dobson, C.M., Hore, P.J., Radford, S.E., Rees, M.L. A photochemically induced dynamic nuclear polarization study of denatured states of lysozyme. Biochemistry 30, 405-412, 1991. doi:10.1021/bi00216a015.

Chatterjee, P., Bagchi, S. and Sengupta, N. The non-uniform early structural response of globular proteins to cold denaturing conditions: a case study with Yfh1. J Chem Phys., 141, 205103, 2014, doi: 10.1063/1.4901897. PMID: 25429964.

Danielsson, J., Mu, X., Lang, L., Wang, H., Binolfi, A., Theillet, F. X., Bekei, B., Logan, D. T., Selenko, P., Wennerström, H. and Oliveberg, M.: Thermodynamics of protein destabilization in live cells, Proc. Natl. Acad. Sci. U. S. A. 112, 12402-7, 2015, doi: 10.1073/pnas.1511308112.

Day, I.J., Maeda, K., Paisley, H.J., Mok, K.H., Hore, P.J. Refolding of ribonuclease A monitored by real-time photo-CIDNP NMR spectroscopy. J Biomol NMR. 44, 77-86, 2009. doi:10.1007/s10858-009-9322-2

Espinosa, Y. R., Grigera, J. R. and Caffarena, E. R. Essential dynamics of the cold denaturation: pressure and temperature effects in yeast frataxin. Proteins, 85, 125-136, 2017, doi: 10.1002/prot.25205. Epub 2016 Nov 20. PMID: 27802581.

Guseman, A. J., Speer, S. L., Perez Goncalves, G. M. and Pielak, G. J.: Surface Charge Modulates Protein-Protein Interactions in Physiologically Relevant Environments, Biochemistry 57, 1681-1684, 2018, doi: 10.1021/acs.biochem.8b00061.

Halle, B. Flexibility and packing in proteins. Proc Natl Acad Sci U S A., 99, 1274-9, 2002, doi: 10.1073/pnas.032522499.

Improta, S., Molinari, H., Pastore, A., Consonni, R. and Zetta, L. Probing protein structure by solvent perturbation of NMR spectra. Photochemically induced dynamic nuclear polarization

464   and paramagnetic perturbation techniques applied to the study of the molten globule state of
465   alpha-lactalbumin. Eur. J. Biochem., 227, 87-96, 1995, doi: 10.1111/j.1432-
466   1033.1995.tb20362.x.

467   Kaptein, R., Dijkstra, K. and Nicolay, K. Laser photo-CIDNP as a surface probe for proteins
468   in solution. Nature, 274, 293-4, 1978, doi:10.1038/274293a0.

469   Kim, P. S. and Baldwin, R. L. Intermediates in the folding reactions of small proteins, Annu.
470   Rev. Biochem., 59, 631-60, 1990, doi: 10.1146/annurev.bi.59.070190.003215.

471   Lyon, C.E., Suh, E.S., Dobson, C.M., Hore, P.J. Probing the exposure of tyrosine and
472   tryptophan residues in partially folded proteins and folding intermediates by CIDNP pulse-
473   labeling. J Am Chem Soc. 124, 13018-13024, 2002, doi:10.1021/ja020141w.

474   Martin, S. R., Esposito, V., De Los Rios, P., Pastore, A. and Temussi, P. A.: The effect of
475   low concentrations of alcohols on protein stability: a cold and heat denaturation study of
476   yeast frataxin, J. Am. Chem. Soc., 130, 9963–9970, 2008, doi: 10.1021/ja803280e.

477   Martin, S. R., Esposito, V., De Los Rios, P., Pastore, A. and Temussi, P. A. The effect of low
478   concentrations of alcohols on protein stability: a cold and heat denaturation study of yeast
479   frataxin. J. Am. Chem. Soc. 130, 9963-70, 2008, doi: 10.1021/ja803280e.

480   Miranker, A., Radford, S. E., Karplus, M. and Dobson, C. M. Demonstration by NMR of
481   folding domains in lysozyme, Nature, 349, 633-6, 1991, doi: 10.1038/349633a0.

482   Miranker, A., Robinson, C. V., Radford, S. E., Aplin, R. T. and Dobson, C. M. Detection of
483   transient protein folding populations by mass spectrometry, Science, 262, 896-900, 1993, doi:
484   10.1126/science.8235611. PMID: 8235611.

485   Monsellier, E. and Bedouelle, H. Quantitative measurement of protein stability from unfolding
486   equilibria monitored with the fluorescence maximum wavelength. Protein Eng. Des. Sel. 18,
487   445-56, 2005, doi: 10.1093/protein/gzi046.

488   Nojima, H., Ikai, A., Oshima, T. and Noda, H.: Reversible thermal unfolding of thermostable
489   phosphoglycerate kinase. Thermostability associated with mean zero enthalpy change, J. Mol.
490   Biol.;116, 429-42, 1977, doi: 10.1016/0022-2836(77)90078-x.

491   Pastore, A. and Temussi, P. A. The Emperor's new clothes: Myths and truths of in-cell NMR.
492   Arch. Biochem. Biophys., 628, 114-122, 2017, doi: 10.1016/j.abb.2017.02.008.

493   Pastore, A., Martin, S. R., Politou, A., Kondapalli, K. C., Stemmler, T. and Temussi, P. A.:
494   Unbiased cold denaturation: low- and high-temperature unfolding of yeast frataxin under
495   physiological conditions, J. Am. Chem. Soc., 129, 5374-5, 2007, doi: 10.1021/ja0714538.

496   Piotto, M., Saudek, V., Sklenár, V.: Gradient-tailored excitation for single-quantum NMR
497   spectroscopy of aqueous solutions, J Biomol NMR. 2, 661-665, 1992

498   Privalov, P. L.: Cold denaturation of proteins, Crit. Rev. Biochem. Mol. Biol., 25, 281-305,
499   1990, doi: 10.3109/10409239009090612.

500   Puglisi, R., Brylski, Alfano, C., Martin, S. R., Pastore, A. & Temussi, P. A.: Thermodynamics
501   of protein unfolding in complex environments: using 2D NMR to measure protein stability
502   curves. Commun. Chem. 3, 100, 2020, doi:10.1038/s42004-020-00358-1

503 Razvi, A. and Scholtz, J. M.: Lessons in stability from thermophilic proteins, Protein Sci. 15,
504 1569-78, 2006, doi: 10.1110/ps.062130306.

505 Roder, H. and Wüthrich, K. Protein folding kinetics by combined use of rapid mixing
506 techniques and NMR observation of individual amide protons. Proteins, 1, 34-42, 1986, doi:
507 10.1002/prot.340010107.

508 Sanfelice, D., Morandi, E., Pastore, A., Niccolai, N. and Temussi, P. A.: Cold Denaturation
509 Unveiled: Molecular Mechanism of the Asymmetric Unfolding of Yeast Frataxin,
510 Chemphyschem. 16, 3599-602, 2015, doi: 10.1002/cphc.201500765.

511 Sanfelice, D., Politou, A., Martin, S. R., De Los Rios, P., Temussi, P. A. and Pastore A. The
512 effect of crowding and confinement: A comparison of Yfh1 stability in different environments
513 Phys. Biol. 10, 045002, 2013, doi: 10.1088/1478-3975/10/4/045002.

514 Sanfelice, D., Puglisi, R., Martin, S. R., Di Bari, L., Pastore, A. and Temussi, P. A.: Yeast
515 frataxin is stabilized by low salt concentrations: cold denaturation disentangles ionic strength
516 effects   from   specific   interactions,   PLoS   One.   9,   e95801,   2014,   doi:
517 10.1371/journal.pone.0095801.

518 Schlörb, C., Mensch, S., Richter, C., Schwalbe, H. Photo-CIDNP reveals differences in
519 compaction of non-native states of lysozyme. J Am Chem Soc. 128, 1802-1803, 2006.
520 doi:10.1021/ja056757d.

521 Smith, A. E., Zhou, L. Z., Gorensek, A. H., Senske, M. & Pielak, G. J. In-cell thermodynamics
522 and a new role for protein surfaces. *Proc. Natl. Acad. Sci. U S A.* **113**, 1725-30 (2016).

523 Vilanova, B., Sanfelice, D., Martorell, G., Temussi, P. A. and Pastore, A. Trapping a salt-
524 dependent unfolding intermediate of the marginally stable protein Yfh1. Front Mol Biosci., 1,
525 13, 2014, doi: 10.3389/fmolb.2014.00013

526

527 **Table 1**. Thermodynamic parameters of all residues

	ΔH (Kcal/mol)	ΔS (Kcal/mol)	ΔCp (Kcal/molK)	Tm(K)	Tc(K)	RAD
61 Val	19.94	0.067	1.58	298.41	273.82	48.20
63 Gln	21.07	0.072	2.24	294.03	275.56	3.64
64 Glu	27.70	0.093	3.30	297.96	281.43	2.52
65 Val	24.30	0.081	2.71	299.73	282.10	0.31
68 Leu	21.01	0.071	3.02	296.52	282.77	0.75
70 Leu	28.54	0.096	3.73	298.15	283.06	2.35
71 Glu	29.09	0.097	3.59	299.79	283.82	7.13
72 Lys	33.11	0.111	3.73	299.59	282.13	6.24
75 Glu	24.30	0.081	2.75	300.01	282.63	2.07
76 Glu	21.81	0.072	2.37	301.19	283.11	0.91
78 Asp	29.03	0.096	3.18	301.13	283.19	0.17
83 His	22.77	0.076	2.21	298.36	278.17	0.16
86 Asp	25.39	0.084	2.62	300.96	281.94	0.27
87 Ser	22.84	0.076	2.42	299.10	280.57	0.34
88 Leu	31.31	0.104	3.38	301.03	282.83	0.04
89 Glu	30.04	0.100	3.36	300.20	282.62	0.20
90 Glu	26.07	0.087	2.50	300.86	280.43	0.52
91 Leu	34.10	0.114	4.19	300.30	284.26	0.16
92 Ser	28.77	0.096	2.93	300.13	280.87	0.15
93 Glu	19.52	0.065	1.97	300.08	280.64	0.61
94 Ala	23.58	0.079	2.55	299.58	281.41	4.10
95 His	18.60	0.062	1.31	300.69	273.12	0.28
97 Asp	23.31	0.078	2.52	299.02	280.85	0.95
98 Cys	22.59	0.076	2.59	297.67	280.51	0.26
99 Ile	22.05	0.074	2.58	298.23	281.41	0.11
101 Asp	22.34	0.074	2.42	300.23	282.09	1.08
104 Leu	29.54	0.098	3.12	300.93	282.34	0.78
105 Ser	27.75	0.092	3.15	300.05	282.72	1.18
107 Gly	19.28	0.065	2.44	296.58	281.00	3.58
108 Val	22.33	0.075	2.03	299.01	277.49	0.50
109 Met	26.64	0.089	3.25	299.41	283.26	0.63
110 Thr	33.20	0.111	3.79	300.20	282.97	0.23
112 Glu	28.52	0.094	2.88	301.86	282.43	0.41
113 Ile	17.44	0.059	2.11	297.57	281.29	0.12
115 Ala	22.32	0.075	4.01	297.04	286.00	2.48
116 Phe	23.03	0.077	3.09	299.15	284.44	0.62
117 Gly	27.62	0.093	3.48	298.20	282.56	0.98
119 Tyr	24.94	0.083	2.72	300.26	282.24	0.22
120 Val	15.70	0.053	1.68	297.29	278.94	0.33
127 Asn	23.00	0.077	2.46	296.97	278.61	5.81
128 Lys	15.54	0.052	1.35	300.36	277.87	0.66
129 Gln	14.27	0.048	1.80	296.82	281.19	0.20
130 Ile	27.87	0.093	3.19	300.92	283.73	0.02
131 Trp	21.74	0.073	2.54	298.55	281.71	0.04
132 Leu	26.43	0.088	3.33	300.68	285.03	0.02
133 Ala	29.63	0.099	3.27	300.17	282.36	0.19
134 Ser	20.31	0.068	2.07	299.70	280.45	0.13
136 Leu	13.22	0.044	1.27	299.25	278.86	0.25
140 Asn	25.41	0.085	2.80	299.43	281.59	0.17
142 Phe	20.94	0.070	3.06	299.27	285.74	0.03
143 Asp	21.86	0.073	2.50	300.24	283.04	0.13
146 Asn	23.64	0.080	3.61	295.03	282.08	2.00
147 Gly	25.22	0.085	2.37	297.81	276.98	4.80
148 Glu	21.59	0.072	2.69	298.80	282.98	1.40
150 Val	22.92	0.076	2.20	300.74	280.33	0.03
151 Ser	22.70	0.076	2.39	299.87	281.22	0.05
152 Leu	32.20	0.107	3.87	300.00	283.61	0.16
154 Asn	21.87	0.074	2.40	295.07	277.17	1.14
158 Leu	29.11	0.096	3.11	301.94	283.55	0.03
159 Thr	29.76	0.099	3.38	300.04	282.72	0.09
160 Asp	23.61	0.078	2.55	301.19	283.00	0.28
161 Ile	15.59	0.052	1.68	300.08	281.85	0.09
163 Thr	21.9	0.073	2.48	300.30	282.93	0.15
166 Val	27.28	0.091	2.81	300.84	281.79	0.06
168 Lys	17.28	0.058	1.93	299.93	282.33	0.16
170 Ile	22.63	0.075	2.11	301.25	280.25	0.31
172 Lys	28.06	0.095	3.84	294.06	279.64	1.5
174 Gln	20.58	0.069	2.20	297.53	279.16	
131 Trp ε1	28.08	0.094	3.34	299.36	282.87	

528